Article

SOURCE DATA | TRANSPARENT PROCESS | OPEN ACCESS

THE EMBO JOURNAL

The EDC4-XRN1 interaction controls P-body dynamics to link mRNA decapping with decay

William R Brothers[1], Farah Ali[1], Sam Kajjo[1] & Marc R Fabian[1,2,3,*]

Abstract

Deadenylation-dependent mRNA decapping and decay is the major cytoplasmic mRNA turnover pathway in eukaryotes. Many mRNA decapping and decay factors are associated with each other via protein–protein interaction motifs. For example, the decapping enzyme DCP2 and the 5'–3' exonuclease XRN1 interact with the enhancer of mRNA-decapping protein 4 (EDC4), a large scaffold that has been reported to stimulate mRNA decapping. mRNA decapping and decay factors are also found in processing bodies (P-bodies), evolutionarily conserved ribonucleoprotein granules that are often enriched with mRNAs targeted for decay, yet paradoxically are not required for mRNA decay to occur. Here, we show that disrupting the EDC4-XRN1 interaction or altering their stoichiometry inhibits mRNA decapping, with microRNA-targeted mRNAs being stabilized in a translationally repressed state. Importantly, we demonstrate that this concomitantly leads to larger P-bodies that are responsible for preventing mRNA decapping. Finally, we demonstrate that P-bodies support cell viability and prevent stress granule formation when XRN1 is limiting. Taken together, these data demonstrate that the interaction between XRN1 and EDC4 regulates P-body dynamics to properly coordinate mRNA decapping with 5′–3′ decay in human cells.

Keywords microRNA; mRNA decapping; mRNA decay; P-bodies; ribonucleoprotein granules
Subject Categories RNA Biology; Translation & Protein Quality
DOI 10.15252/embj.2023113933 | Received 3 March 2023 | Revised 19 July 2023 | Accepted 22 July 2023 | Published online 25 August 2023
The EMBO Journal (2023) 42: e113933
See also: **LE Malsick & J Wilusz** (November 2023)

Introduction

Translation and mRNA stability are tightly controlled to post-transcriptionally regulate gene expression. In eukaryotes, the majority of cytoplasmic mRNA decay occurs through a deadenylation-dependent program, which involves the removal of the poly(A) tail from the 3′ end of the mRNA (Jonas & Izaurralde, 2015). This is accomplished by deadenylase machineries, including the PAN2-PAN3 and CCR4-NOT deadenylase complexes. Multiple mRNA repression programs directly recruit the CCR4-NOT complex to the 3′-untranslated regions (UTRs) of targeted mRNAs through various 3′UTR-binding proteins. For example, microRNA (miRNA) target sites associate with the miRNA-induced silencing complex (miRISC), which recruits the CCR4-NOT complex to initiate mRNA deadenylation (Fabian *et al*, 2010; Braun *et al*, 2011; Collart & Panasenko, 2012; Jonas & Izaurralde, 2015). Following deadenylation, the mRNA decapping complex is recruited to the 5′-terminus of the mRNA (Yamashita *et al*, 2005). This includes the DCP2-decapping enzyme, the decapping cofactor DCP1, and enhancer of decapping proteins such as EDC3 and EDC4 (Chang *et al*, 2014, 2019; Vidya & Duchaine, 2022), which function to hydrolyze the N^7-methylguanosine 5′-cap structure. Following hydrolysis of the 5′-cap, the mRNA is vulnerable to degradation by the 5′–3′ exonuclease XRN1, which physically associates with the mRNA-decapping complex (Braun *et al*, 2012; Chang *et al*, 2014).

Deadenylation, decapping, and decay factors interact with each other via a complex network of multivalent protein–protein interactions, which can act to support mRNA turnover (Jonas & Izaurralde, 2013). In addition, proteins with described roles in mRNA decay and translational repression can be spatially organized in cytoplasmic ribonucleoprotein (RNP) granules known as processing bodies (P-bodies). P-bodies are dynamic structures that form through complex networks of protein–protein, protein-RNA, and RNA–RNA interactions between RNA-binding proteins and their cognate mRNAs (Standart & Weil, 2018). Indeed, several mRNA decapping and decay factors act as core nucleating proteins critical for visible P-body formation. These include EDC4, DEAD-box helicase 6 (DDX6), the eIF4E-binding protein 4E-T, or like Sm14 (LSM14) (Parker & Sheth, 2007; Franks & Lykke-Andersen, 2008; Jonas & Izaurralde, 2013). For example, LSM14 directly interacts with EDC4, 4E-T, and DDX6, and disrupting any of these interactions prevents visible P-body assembly (Brandmann *et al*, 2018).

Despite being highly concentrated in mRNA decay factors, P-bodies are enigmatic in that they are not required for mRNA decay to occur (Eulalio *et al*, 2007b). Recently, several groups have made correlative observations that suggest there may be a link between P-bodies and the negative regulation of mRNA decapping and 5′ to 3′ decay. These include transcriptomic analyses which show that the classes of mRNAs that localize to P-bodies are typically targeted by

1 Lady Davis Institute for Medical Research, Jewish General Hospital, Montreal, QC, Canada
2 Department of Biochemistry, McGill University, Montreal, QC, Canada
3 Department of Oncology, McGill University, Montreal, QC, Canada
*Corresponding author. Tel: +1 (514) 340 8222 (extn) 28575; E-mail: marc.fabian@mcgill.ca

mRNA decay programs (Hubstenberger *et al*, 2017). However, these analyses also suggest that mRNAs purified directly from P-bodies are protected from 5′ to 3′ decay. These observations are in line with *in vitro* studies of phase-separated yeast DCP1-DCP2 proteins which show that biomolecular condensation can inhibit DCP2 pyrophosphatase activity (Tibble *et al*, 2021). However, whether P-body condensates regulate mRNA decay pathways in cells is still unknown.

mRNA-decapping complex subunit stoichiometry has also been linked to P-body assembly. Interestingly, however, while mRNA decapping is disrupted by depleting cells of any of the mRNA-decapping complex subunits, individual subunit depletion can lead to disparate effects on P-body formation. For instance, EDC4 is a core P-body protein that when depleted leads to the loss of P-bodies (Eulalio *et al*, 2007a, 2007b; Aizer *et al*, 2013; Luo *et al*, 2018). Conversely, depleting cells of DCP2 or XRN1 results in an increase in P-body size in *Drosophila* and yeast cells (Sheth & Parker, 2003; Eulalio *et al*, 2007b). However, despite these observations, direct mechanistic evidence to support a role for P-bodies in regulating mRNA decapping and decay is lacking. Moreover, precisely what regulates the coordination between mRNA decapping and 5′ to 3′ decay in human cells remains unknown.

Here, we set out to elucidate how changes in the levels of mRNA-decapping complex subunits regulate miRNA-mediated mRNA decay. Interestingly, we observe that altering the stoichiometry of EDC4 and XRN1 results in a shift in the mode of miRNA silencing from mRNA decay to translational repression. Specifically, we show that upregulating EDC4 levels, depleting XRN1, or disrupting the ability of EDC4 to interact with XRN1 generates larger P-bodies. We go on to show that the enlarged P-bodies directly stabilize miRNA-targeted mRNAs by inhibiting mRNA decapping under these conditions. Finally, we demonstrate that P-bodies can provide a fitness advantage in the absence of XRN1, as disrupting P-body formation in XRN1 knockout cells leads to stress granule formation and reduces cell viability. Taken together, our data support a model where the EDC4-XRN1 interaction regulates mRNA-decapping activity through P-body formation, which feeds back on cell viability when XRN1 is limiting.

Results

Elevated EDC4 levels shift the mode of miRNA-mediated silencing from mRNA decay to translational repression by remodeling P-bodies

The depletion of EDC4 has been linked to a loss of mRNA-decapping activity and decay (Erickson *et al*, 2015). Therefore, we hypothesized that increasing cellular EDC4 levels might enhance the decay of a miRNA-targeted reporter. To test this, EDC4-overexpressing HeLa cells were transfected with plasmids encoding a *Renilla* luciferase (RL) reporter mRNA with six *let-7* miRNA target sites (RL-6xB) or six mutated let-7 sites (RL-6xBMUT) in its 3′UTR (Fig 1A and B) (Fabian *et al*, 2009). Forty-eight hours post-transfection, cells were lysed and RL-6xB silencing was measured using luciferase assays, with RL-6xBMUT serving as a control. In addition, RL-6xB and RL-6xBMUT mRNA stability was assessed by actinomycin D (Act-D) treatment to inhibit transcription, isolation of total RNA at multiple time points, and measurement of mRNA levels by reverse transcription-quantitative PCR (RT–qPCR). Overexpression of EDC4 did not significantly alter the extent of RL-6xB repression as determined by luciferase assays (Fig 1C). Surprisingly, however, while RL-6xB mRNA rapidly degraded in cells expressing only endogenous EDC4, RL-6xB mRNA was stabilized in EDC4-overexpressing cells with a decay rate similar to that of the RL-6xBMUT control mRNA (Fig 1D). Additionally, mRNA decay assays were performed using RL-6xB and RL-6xBMUT reporters that can be transcriptionally inhibited upon the addition of doxycycline (Fig EV1A) (Urlinger *et al*, 2000). In keeping with our previous observations, RL-6xB mRNAs were more stable in EDC4-overexpressing cells relative to control cells, suggesting that the effects of EDC4 on mRNA stability are not dependent on inhibiting global transcription.

Next, we wondered why elevated EDC4 levels would lead to the stabilization of a miRNA-targeted mRNA. Previously, we showed that EDC4 overexpression in HeLa cells leads to a dramatic increase in P-body size (Fig 1E and F) (Brothers *et al*, 2020, 2022). Recent single-molecule imaging studies point to P-bodies serving as "waystations" for the persistent translational repression of mRNAs targeted by the miRISC (Cialek *et al*, 2022). Moreover, several lines of evidence suggest that mRNAs within P-bodies are not actively undergoing decay (Eulalio *et al*, 2007b; Arribere *et al*, 2011; Hubstenberger *et al*, 2017; Di Stefano *et al*, 2019). Therefore, we next wanted to determine if EDC4-remodeled P-bodies play a role in stabilizing the RL-6xB mRNA. To this end, we targeted the core P-body protein LSM14A using CRISPR-Cas9 to generate knockout LSM14A HeLa cells (LSM14A^{KO}) and then stably rescued LSM14A expression with wild-type FLAG-tagged LSM14A (F-LSM14A^{WT}) or LSM14A mutants that do not interact with EDC4 (F-LSM14A$^{\Delta FFD}$) or DDX6 (F-LSM14A$^{\Delta TFG}$) (Fig 2A and B) (Brandmann *et al*, 2018). Importantly, these LSM14A mutants do not support visible P-bodies, even when EDC4 is overexpressed (Fig 2C) (Brothers *et al*, 2022). Cells were transfected with RL-6xB and RL-6xBMUT reporter constructs alone or with a plasmid-encoding V5-tagged EDC4. We found that RL-6xB was repressed equally well in F-LSM14A^{WT} or F-LSM14A$^{\Delta FFD}$ cells as assessed by luciferase assays, regardless of EDC4 overexpression (Fig 2D). However, while RL-6xB mRNA was stabilized in F-LSM14A^{WT} cells that expressed high levels of EDC4, it rapidly decayed in F-LSM14A$^{\Delta FFD}$ and F-LSM14A$^{\Delta TFG}$ cells that lack P-bodies (Fig 2E). We also examined the decay rates of *MCL1* and *BCL2*, two endogenous mRNAs that are targeted by deadenylation-dependent decay programs, and are reported to be enriched in P-bodies (Ishimaru *et al*, 2010; Hubstenberger *et al*, 2017; Cui & Placzek, 2018). Like RL-6xB, EDC4 overexpression stabilized both *MCL1* and *BCL2* mRNAs in F-LSM14A^{WT} cells but had no effect in LSM14A$^{\Delta FFD}$ cells with both transcripts decaying in a rapid manner (Figs 2F and EV1B and C). Moreover, consistent with our luciferase assays (Fig 1C), EDC4 overexpression had no impact on the steady-state levels of MCL1 and BCL2 proteins in WT HeLa cells (Fig EV1D). Using an alternative approach, we disrupted P-bodies using NBDY, a microprotein that interacts with EDC4 and DCP1A and promotes P-body dissociation (Fig 3A and B) (D'Lima *et al*, 2017; Na *et al*, 2020, 2021; Brothers *et al*, 2022). Expressing NBDY in EDC4-overexpressing cells also restored the decay rates and half-lives of exogenously introduced RL-6xB, or endogenous *MCL1* and *BCL2* mRNAs to rates similar to those observed in control cells (Figs 3C–E and EV1E). Taken together, our results indicate that upregulating EDC4 remodels P-body condensates, which in turn is

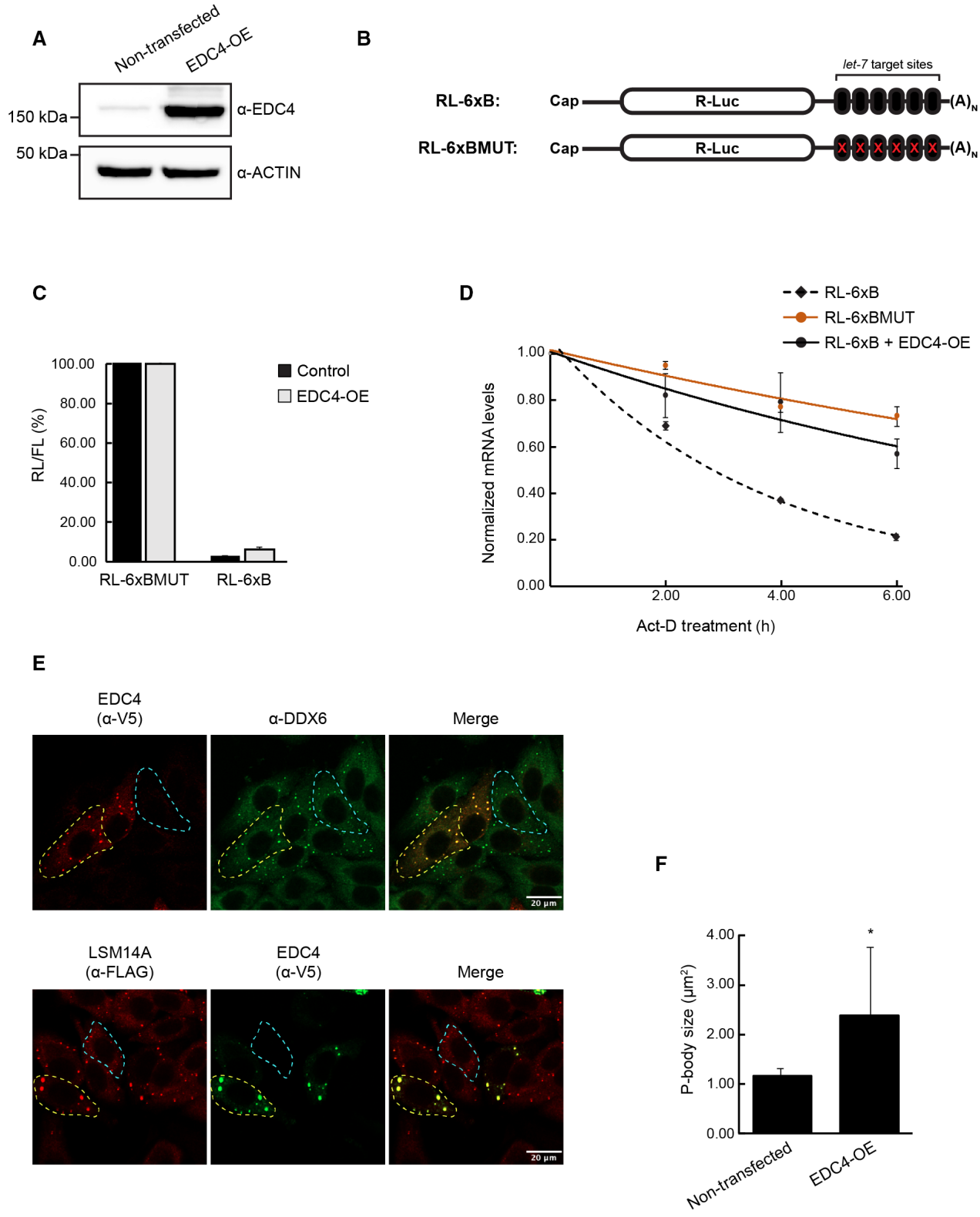
A
Non-transfected
EDC4-OE
150 kDa
α-EDC4
50 kDa
α-ACTIN
B
let-7 target sites
RL-6xB:
Cap
R-Luc
(A)N
RL-6xBMUT:
Cap
R-Luc
(A)N
C
RL/FL (%)
100.00
80.00
60.00
40.00
20.00
0.00
Control
EDC4-OE
RL-6xBMUT
RL-6xB
D
RL-6xB
RL-6xBMUT
RL-6xB + EDC4-OE
Normalized mRNA levels
1.00
0.80
0.60
0.40
0.20
0.00
2.00
4.00
6.00
Act-D treatment (h)
E
EDC4 (α-V5)
α-DDX6
Merge
20 μm
LSM14A (α-FLAG)
EDC4 (α-V5)
Merge
20 μm
F
P-body size (μm2)
4.00
3.00
2.00
1.00
0.00
*
Non-transfected
EDC4-OE

Figure 1.

Figure 1. EDC4 levels enhance P-body condensation and stabilize miRNA-targeted mRNAs.

A Western blot validation of EDC4 overexpression.

B Schematic diagrams of *Renilla* luciferase reporter mRNAs with six *let-7* (RL-6xB) or mutated *let-7* (RL-6xBMUT) target sites.

C Luciferase assays performed on HeLa cells expressing the indicated reporters with or without EDC4-overexpression. Luciferase values are expressed as an RL/FL ratio with the RL/FL ratio of RL-6xBMUT-expressing cells normalized to 100%. Error bars represent the SEM of three biological replicates.

D mRNA decay assay assessing the decay rates of cells expressing the indicated reporters and proteins. RNA was isolated from cells after treatment with actinomycin D (Act-D) to halt transcription. mRNA levels were measured by RT–qPCR with RL-6xB levels being normalized to *GAPDH* levels. Normalized RL-6xB levels at 0 h of Act-D treatment were set to 1.0. Error bars represent the SEM of three biological replicates.

E Images generated through confocal microscopy of HeLa cells transfected with plasmids encoding EDC4-V5. Immunofluorescent staining was performed using α-V5 and antibodies to detect the P-body markers DDX6 and LSM14A. Images were processed, and channels were merged using Fiji. Yellow outlines highlight cells that have been transfected with the indicated proteins, in contrast to non-transfected cells (blue outlines).

F Quantification of P-body sizes in cells transfected with EDC4-V5 compared to non-transfected controls in the same samples. Measurements were performed on three separate biological replicates using Fiji. Error bars represent the SEM and statistical significance was established using a two-tailed Student's *t*-test (*$P < 0.05$).

Source data are available online for this figure.

responsible for shifting the mode of mRNA silencing from mRNA decay to translational repression.

EDC4 overexpression enriches stabilized miRNA-targeted mRNAs within P-bodies

Both exogenously introduced reporters and endogenous mRNAs targeted by miRNAs have been reported to localize to P-bodies (Liu *et al*, 2005; Hubstenberger *et al*, 2017). As our data indicate that overexpressing EDC4 stabilizes a miRNA-targeted mRNA by enhancing P-body formation, we next wanted to determine if miRNA-targeted mRNAs are differentially localized to P-bodies under these conditions. To assess this, we transfected F-LSM14A^{WT} HeLa cells with plasmid-encoding RL-6xB alone or with plasmids that overexpress V5-tagged EDC4 and performed fluorescent *in situ* hybridization (FISH) using Cy3-labeled probes against the RL-6xB reporter mRNA. To establish whether the FISH signal co-localizes to *bona fide* P-bodies, we performed simultaneous immunofluorescent staining against DDX6 and either LSM14A (α-FLAG) when EDC4 was not overexpressed or V5-EDC4 (α-V5) in EDC4-overexpressing cells (Fig 4A). As overexpressing EDC4 stabilized RL-6xB mRNA in cells that form visible P-bodies, we also treated transfected cells with Act-D for 4 h to investigate whether RL-6xB mRNAs are differentially stabilized within EDC4-remodeled P-bodies (Fig 4B). P-bodies, as defined by the punctate signal overlap between the two protein channels, were approximately twofold larger in EDC4-overexpression conditions (Fig 4C). We also stained for the stress granule marker G3BP1, which remained diffuse throughout the cytoplasm and did not overlap with RL-6xB FISH signal (Fig EV2A), indicating that EDC4 overexpression does not lead to stress granule formation.

Next, we quantified the overall FISH signal from cells expressing RL-6xB. Consistent with our results from mRNA stability assays (Fig 1F), RL-6xB FISH signal was significantly elevated in EDC4-overexpressing cells after 4 h of Act-D treatment compared to cells expressing only endogenous EDC4 (Fig 4D). Additionally, we found significant enrichment of RL-6xB signal overlapping with P-bodies upon EDC4 overexpression relative to cells with endogenous EDC4 (Fig 4E). In contrast to the RL-6xB, RL-6xBMUT mRNA displayed a diffuse localization pattern, suggesting that the presence of *let-7* miRNA target sites is required for P-body localization (Fig EV2B). It is important to note that cells treated with Act-D exhibited fewer but larger P-bodies than untreated cells, as has been reported previously (Cougot *et al*, 2004). Therefore, we also measured the mean RL-6xB signal per individual P-body to normalize for differences in P-body numbers between conditions (Fig 4F). This analysis showed that Act-D treatment was associated with higher RL-6xB signal per P-body in both control and EDC4-overexpressing cells, indicating that mRNAs enriched in P-bodies are being preferentially protected from degradation. Together, these results suggest that RL-6xB mRNAs are enriched within P-bodies due to EDC4 overexpression, leading to their protection from decay.

miRNA-targeted mRNAs stabilized in P-bodies are deadenylated but not decapped

miRNA-targeted mRNAs are generally destabilized via deadenylation, followed by decapping and subsequent 5′ to 3′ decay (Jonas & Izaurralde, 2015). Our data suggest that the decay of the *let-7*-targeted RL-6xB mRNA is impaired when EDC4 enhances P-body condensates. We therefore set out to identify what step in the mRNA decay pathway is inhibited under these conditions. To assess the poly(A) tail status of RL-6xB mRNA in EDC4-overexpressing cells, we isolated total RNA at 0 and 6 h following Act-D treatment and performed enhanced poly(A)-tailing (ePAT) assays (Jänicke *et al*, 2012) (Fig 5A). While RL-6xB mRNA displayed long heterogeneous poly(A) tails at the 0-h time point, it maintained a short poly (A) tail after 6 h of Act-D treatment, suggesting that these mRNAs are being actively targeted for deadenylation. This contrasts with *GAPDH* mRNAs, which are also stable but maintain heterogeneous poly(A) tail lengths at both 0 and 6 h of Act-D treatment. To determine the RL-6xB mRNA-cap status in EDC4-overexpressing cells, we incubated RNA isolated from cells treated with Act-D for 6 h with Terminator nuclease, a 5′–3′ exonuclease that degrades uncapped RNAs with a 5′ monophosphate (Braun *et al*, 2012). Following Terminator treatment, total RNA was isolated and RNA levels were quantified by RT–qPCR with spike-in RNA for normalization (Fig 5B). The Terminator nuclease failed to efficiently degrade RL-6xB mRNA from samples collected after 6 h of Act-D treatment, as these mRNAs were reduced to similar degrees as *GAPDH* mRNA. In contrast, the Terminator nuclease efficiently degraded 18S rRNA, which does not harbor a 5′-cap. However, RL-6xB mRNA levels were further reduced by Terminator nuclease when we first treated RNA *in vitro* with an mRNA-decapping enzyme (Paquette *et al*, 2018) (Fig EV3A). These results suggest that enhanced P-body formation prevents miRNA-targeted mRNAs from being decapped after they have been deadenylated.

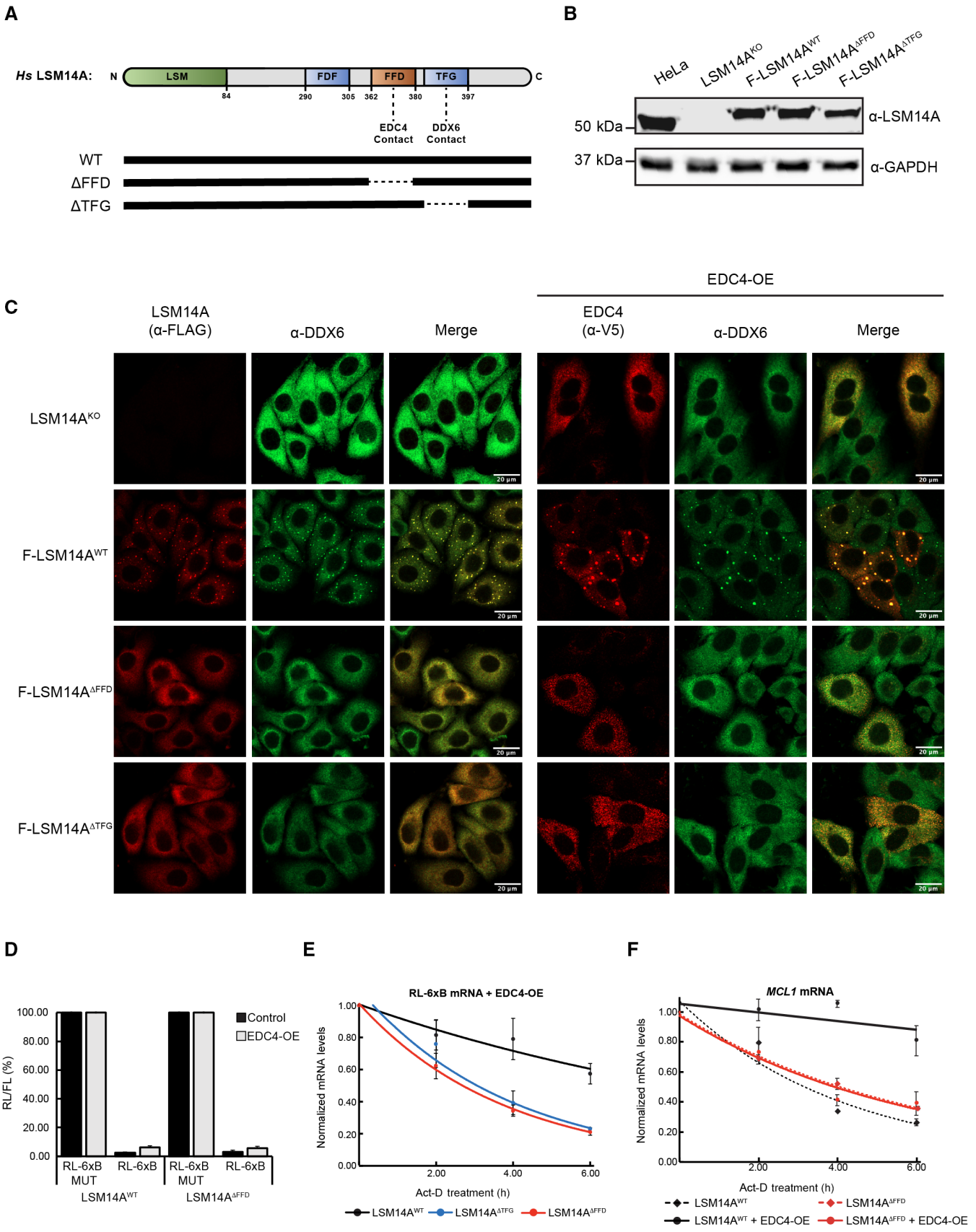

Figure 2.

Figure 2. P-bodies bias miRNA silencing from target mRNA decay to translational repression.

A Schematic diagram of human LSM14A, along with diagrams representing deletion mutants that disrupt P-body formation.

B Western blotting of WT or LSM14^{KO} HeLa cells stably rescued with FLAG-tagged (F-)LSM14A proteins.

C Images generated through confocal microscopy of LSM14A^{KO} HeLa cells stably expressing F-LSM14A constructs under endogenous EDC4 expression or EDC4 overexpression. Immunofluorescent staining was performed using α-FLAG under endogenous EDC4 expression levels or α-V5 under EDC4 overexpression with α-DDX6. Images were processed, and channels were merged using Fiji.

D Luciferase assays performed on LSM14A^{WT} or LSM14A$^{\Delta FFD}$ cells expressing the indicated reporters with or without EDC4 overexpression (EDC4-OE). Luciferase values are expressed as an RL/FL ratio with the RL/FL ratio of RL-6xBMUT-expressing cells normalized to 100%. Error bars represent the SEM of three biological replicates.

E, F mRNA decay assays in the indicated F-LSM14 cell lines assessing the decay rates of miRNA-targeted mRNAs with or without EDC4-OE. RNA was isolated from cells after treatment with actinomycin D (Act-D) to halt transcription. mRNA levels were measured by RT–qPCR with RL-6xB (E) or *MCL1* (F) levels being normalized to *GAPDH* levels. Normalized RL-6xB (E) or *MCL1* (F) levels at 0-h of Act-D treatment were set to 1.0. Error bars represent the SEM of three biological replicates.

Source data are available online for this figure.

Depleting XRN1 inhibits mRNA decapping by enhancing P-body condensation

Our data suggest that enhancing P-body formation by upregulating EDC4 levels limits mRNA decapping in human cells. It has previously been shown that depleting XRN1 in yeast and *Drosophila* S2 cells lead to similarly enlarged P-bodies (Sheth & Parker, 2003; Eulalio *et al*, 2007b), a phenotype that we also observe in XRN1^{KO} HeLa cells compared to WT HeLa cells (Fig 6A–C). Moreover, in *Drosophila* S2 cells, depletion of XRN1 has been reported to inhibit mRNA decapping via an unknown mechanism (Braun *et al*, 2012). We therefore aimed to determine if loss of XRN1 impairs mRNA decapping in human cells, and if this effect is mediated by alterations in P-body condensation. To test this, we introduced the RL-6xB reporter into WT and XRN1^{KO} HeLa cells alone or with a plasmid-encoding FLAG-tagged NBDY to disrupt visible P-bodies formation (Fig 6D and E). Cells were treated with Act-D for 6 h to inhibit *de novo* transcription and total RNA was isolated to assess both mRNA stability and 5′-cap status, the latter by incubating isolated RNA with Terminator nuclease (Fig 6F and G). RL-6xB mRNA was significantly more stable in XRN1^{KO} cells compared to WT cells, regardless of NBDY expression (Fig 6F). However, Terminator nuclease failed to degrade RL-6xB mRNA from XRN1^{KO} cells, but efficiently degraded RL-6xB mRNA from NBDY-expressing XRN1^{KO} cells (Fig 6G). The efficient degradation of ribosomal RNA by Terminator nuclease under both conditions suggests that the differences in RL-6xB mRNA degradation were not caused by changes in Terminator nuclease activity. We also performed RNA immunoprecipitation (RIP) analyses to assess the relative levels of capped mRNAs in XRN1^{KO} cells with or without P-bodies. To this end, XRN1^{KO} cells were transfected with plasmids encoding the RL-6xB reporter with or without FLAG-NBDY and treated with Act-D for 6 h. Total RNA was then extracted, and capped mRNAs were immunopurified using an antibody against m^{7}G. We observed strong enrichments of capped RL-6xB, *MCL1*, *BCL2*, and *GAPDH* mRNAs relative to 18S rRNA in all m^{7}G RIP samples when compared to inputs (Fig EV3B). Moreover, NBDY expression led to a significant reduction in the enrichment of the capped mRNAs that are known to be enriched within P-bodies (i.e., RL-6xB, *MCL1*, and *BCL2*), but did not reduce the levels of capped *GAPDH* transcripts (Fig 6H). Taken together, these results indicate that loss of XRN1 has a similar effect to overexpressing EDC4, resulting in impaired mRNA decapping by enhancing P-body formation in human cells.

The EDC4-XRN1 interaction coordinates mRNA decapping with decay in human cells

One possible explanation for why we observe enlarged P-bodies in XRN1^{KO} cells is that increasing the stability of P-body-enriched mRNAs provides P-body proteins with more mRNA to aggregate with, increasing multivalency for condensate formation. To test this hypothesis, we transfected XRN1^{KO} cells with the RL-6xB reporter, along with plasmids encoding FLAG-tagged wild-type XRN1 (F-XRN1^{WT}) or a catalytically inactive XRN1 mutant (F-XRN1^{E178Q}) that cannot promote mRNA decay (Chang *et al*, 2011) (Figs 7A and EV3C–E). As anticipated, F-XRN1^{WT} rescued RL-6xB mRNA decay, whereas F-XRN1^{E178Q} failed to do so (Fig 7B). However, both F-XRN1^{WT} and F-XRN1^{E178Q} similarly restored P-body size (Figs 7C and EV3F) and rescued mRNA decapping as assessed by Terminator nuclease assays (Fig 7D). This indicates that XRN1 does not require its exonuclease activity to promote P-body formation and enhance mRNA decapping.

The Izaurralde Lab previously demonstrated that XRN1 coordinates mRNA decapping and decay in *Drosophila* by directly binding to DCP1 (Braun *et al*, 2012). In contrast, while human XRN1 also interacts with mRNA-decapping factors, it does not directly interact with DCP1. Rather, XRN1 associates with the mRNA-decapping complex using a conserved C-terminal EDC4-binding motif (EDC4-BM) in human cells (Braun *et al*, 2012; Chang *et al*, 2014) (Fig 7A). As our data show that modulating the levels of EDC4 or XRN1 regulates mRNA decapping by altering P-body formation, we next tested whether the EDC4-XRN1 interaction is responsible for regulating these processes in human cells. To this end, we complemented XRN1^{KO} cells with the XRN1 catalytic domain alone (F-XRN1^{MUT1}), which lacks the EDC4-binding motif (EDC4-BM) (Figs 7A and EV3E). However, this mutant failed to restore P-body size or promote RL-6xB mRNA decapping and decay (Figs 7B–D and EV3F). On the other hand, fusing the XRN1 catalytic domain to the EDC4-BM (F-XRN1^{MUT2}) restored P-body size and reestablished RL-6xB mRNA destabilization to levels seen with F-XRN1^{WT} rescue (Fig 7B and C). Importantly, a nuclease-dead version of this construct (F-XRN1^{MUT3}) failed to rescue RL-6xB mRNA decay but restored both P-body size and RL-6xB mRNA decapping as assessed via Terminator nuclease assays (Figs 7B–D and EV3F). Collectively, these data indicate that the interaction between EDC4 and XRN1 regulates P-body formation, which in turn coordinates mRNA decapping and decay in human cells.

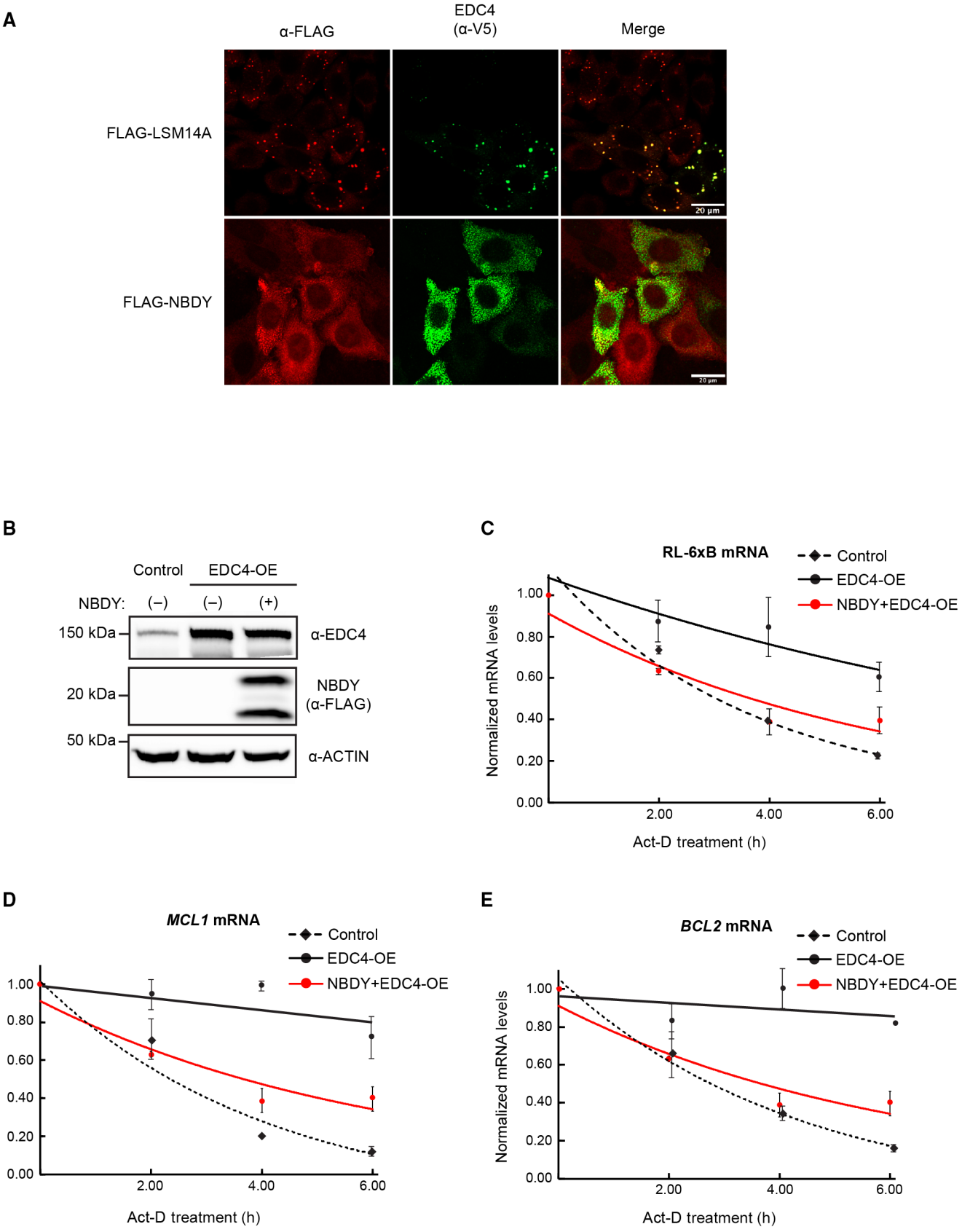
A
α-FLAG
EDC4
(α-V5)
Merge
FLAG-LSM14A
FLAG-NBDY
20 μm
B
Control
EDC4-OE
NBDY: (–) (–) (+)
150 kDa
α-EDC4
20 kDa
NBDY
(α-FLAG)
50 kDa
α-ACTIN
C
RL-6xB mRNA
Control
EDC4-OE
NBDY+EDC4-OE
Normalized mRNA levels
Act-D treatment (h)
D
MCL1 mRNA
E
BCL2 mRNA

Figure 3.

Figure 3. NBDY negates the effects of EDC4 overexpression (EDC4-OE) on miRNA-mediated decay rates.

A Images generated through confocal microscopy of HeLa cells transfected with plasmids encoding EDC4-V5 and FLAG-NBDY. Immunofluorescent staining was performed using α-FLAG and α-V5 antibodies. Images were processed, and channels were merged using Fiji.

B Western blots of HeLa cell extracts expressing the indicated proteins.

C–E mRNA decay assay assessing the decay rates of miRNA-targeted mRNAs with or without EDC4-OE. RNA was isolated from cells after treatment with actinomycin D (Act-D) to halt transcription. mRNA levels were measured by RT–qPCR with RL-6xB (C), *MCL1* (D), or *BCL2* (E) levels being normalized to *GAPDH* levels. Normalized RL-6xB (C), *MCL1* (D), or *BCL2* (E) levels at 0-h of Act-D treatment were set to 1.0. Error bars represent the SEM of three biological replicates.

Source data are available online for this figure.

P-bodies support cell viability in the absence of XRN1

Stress granules are RNP granules that form in response to a variety of cellular stresses including oxidative stress, viral infection, and amino acid starvation, and contain several proteins that are also found in P-bodies (Beckham & Parker, 2008; Protter & Parker, 2016). We observed that overexpressing EDC4 or knocking out XRN1 led to an increase in P-body size. However, while overexpressing EDC4 did not lead to the formation of G3BP1-positive stress granules (Fig EV2A), we observed a small percentage (~5%) of XRN1^{KO} cells that contained stress granules, even though they were not exposed to cellular stressors (Fig 8A). One possible explanation for this is that altered P-body morphology in the absence of XRN1 can lead to low levels of cellular stress, which in turn results in stress granule formation. To test this, we expressed NBDY in XRN1^{KO} cells to disrupt P-body formation and determine whether this might attenuate stress granule formation. Incredibly, expressing NBDY in XRN1^{KO} HeLa cells led to a dramatic increase in stress granule formation, with the majority of cells displaying G3BP1-positive stress granules staining for NBDY expression (Fig 8B and C). In contrast, we did not observe stress granules forming in NBDY-expressing wild-type cells (Fig 8B, top panels). Importantly, disrupting P-body formation led to a significant decrease in viability of XRN1^{KO} cells but had no impact on wild-type cell viability (Fig 8D). Furthermore, these observations are specifically due to the loss of XRN1, as rescuing XRN1 levels in XRN1^{KO} cells with exogenous F-XRN1^{WT} prevented stress granules from forming (Fig 8A) and rescued their viability in the absence of visible P-bodies (Fig 8D). Thus, these data demonstrate that P-bodies support cell viability in the absence of XRN1 and prevent the formation of stress granules in the absence of external stress.

Discussion

Descriptions of a mechanistic role(s) for P-bodies in regulating mRNA stability have been historically elusive. In this study, we present data that support a model whereby P-bodies regulate mRNA decapping in response to changes in mRNA decapping and decay factor stoichiometry (Fig 8E). We show that enhancing P-body formation by overexpressing EDC4, depleting XRN1, or disrupting the EDC4-XRN1 interaction impairs mRNA decapping of P-body-enriched mRNAs. Together, our data point to a model whereby EDC4-XRN1 stoichiometry and their association feed back on mRNA-decapping activity by modulating P-body morphology. Moreover, our data suggest that enhanced P-body formation in the absence of XRN1 attenuates stress granule formation and promotes cellular fitness. To our knowledge, this study is the first to directly attribute a mechanistic function to P-bodies in the post-transcriptional regulation of gene expression.

Transcriptomic analyses of P-body-enriched mRNAs demonstrate that they are mainly comprised of poorly translated mRNAs that are targeted for decay by RNA-binding proteins via *cis*-regulatory elements (Hubstenberger *et al*, 2017; Matheny *et al*, 2019). However, these analyses suggest that mRNAs within P-bodies are not actively undergoing decay. Importantly, sequencing read distribution of transcripts purified directly from P-bodies was significantly shifted toward the 5′end of the mRNAs relative to the total and P-body-depleted transcriptomes, suggesting that they are being protected from 5′ to 3′ decay (Hubstenberger *et al*, 2017). In line with these observations, our results show that P-bodies can be remodeled to impair mRNA decapping, leading to further mRNA enrichment within P-bodies that protects them from 5′ to 3′ decay. However, precisely how P-bodies block mRNA decapping remains unknown. *In vitro* studies using recombinant yeast DCP1 and DCP2 proteins suggest that liquid–liquid phase separation can bias DCP2 conformation to impair its pyrophosphatase activity (Tibble *et al*, 2021). P-granules in *C. elegans* germ cells—structures compositionally similar to P-bodies—have been shown to exhibit liquid-like behaviors that rapidly dissolve and condense (Brangwynne *et al*, 2009). Therefore, P-body phase transitions may alter DCP2 conformation or localization *in vivo*, which could explain how P-body aggregation inhibits mRNA decapping. Another plausible explanation is that P-bodies serve as a physical barrier that limits DCP2 from interfacing with its target mRNAs. In support of the latter hypothesis, mRNAs targeted by DCP2 are disproportionately enriched within P-bodies (Luo *et al*, 2020). Moreover, a large proportion of DCP2-target mRNAs are also stabilized by knocking out NBDY, which leads to increases in the number and sizes of P-bodies (Na *et al*, 2020). Therefore, enhanced P-body enrichment of DCP2 target mRNAs may be what prevents their decapping. Nevertheless, additional research is needed to determine the structural underpinnings of mRNA-decapping regulation by P-bodies *in vivo*.

We have shown that the EDC4-XRN1 interaction is a key regulator of P-body size and mRNA-decapping activity. XRN1^{KO} human cells exhibit significantly larger P-bodies and deficits in decapping of miRNA-targeted mRNAs, both of which can be rescued by XRN1 variants that re-establish contact with EDC4—irrespective of XRN1 exoribonuclease activity. These results are in line with studies from the Izarraulde Lab, which showed that an XRN1 mutant that cannot bind EDC4 failed to degrade a reporter mRNA targeted by the nonsense-mediated decay protein SMG7 in human cells (Chang *et al*, 2019). Although they did not assess whether this XRN1 mutant failed to degrade the SMG7-targeted reporter due to deficits in mRNA-decapping activity, their previous work demonstrated that the DCP1-XRN1 interaction is required for efficient mRNA

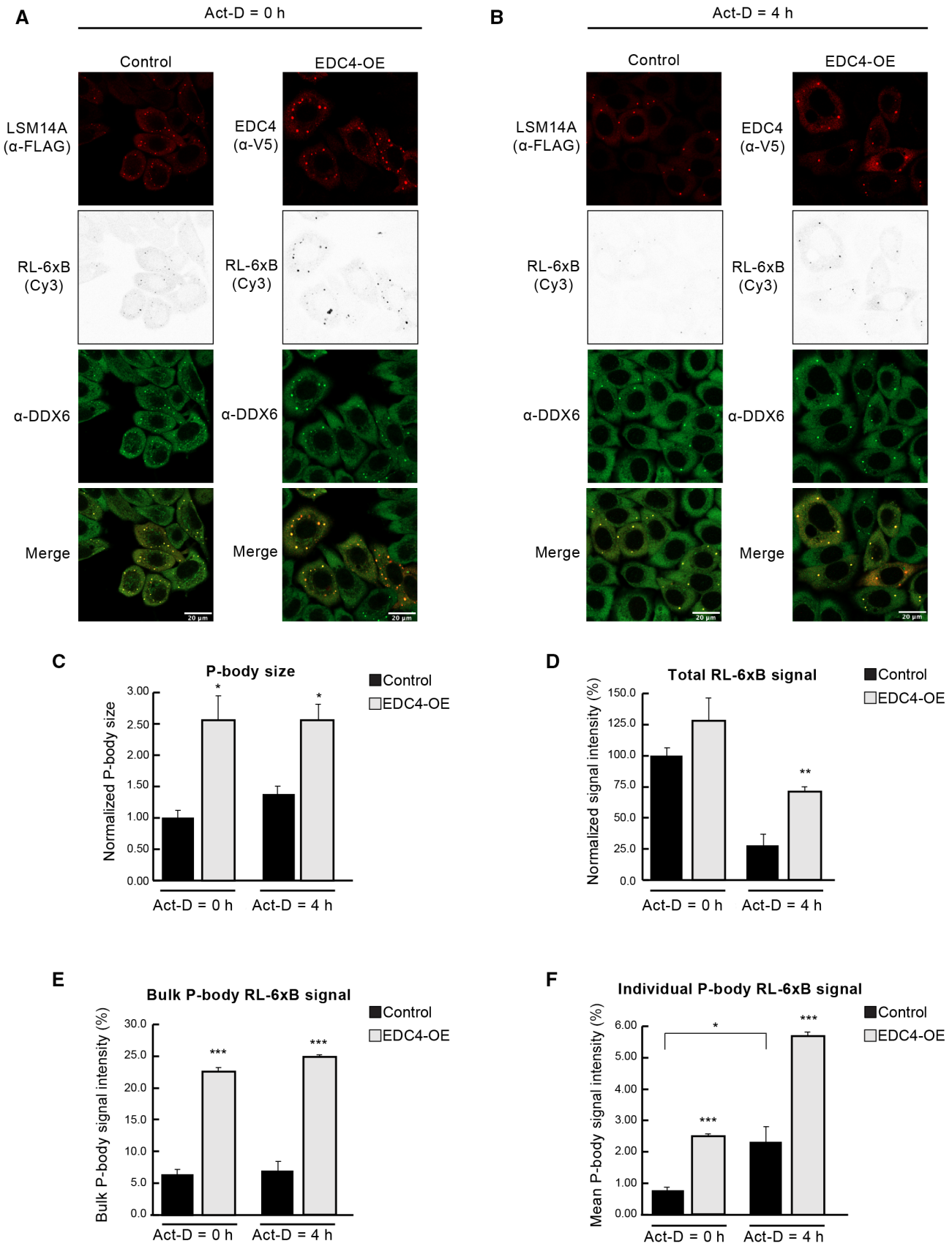
A
Act-D = 0 h
Control
EDC4-OE
LSM14A (α-FLAG)
EDC4 (α-V5)
RL-6xB (Cy3)
α-DDX6
Merge
20 μm
B
Act-D = 4 h
C
P-body size
Normalized P-body size
Control
EDC4-OE
Act-D = 0 h
Act-D = 4 h
D
Total RL-6xB signal
Normalized signal intensity (%)
E
Bulk P-body RL-6xB signal
Bulk P-body signal intensity (%)
F
Individual P-body RL-6xB signal
Mean P-body signal intensity (%)

Figure 4.

Figure 4. EDC4 overexpression differentially recruits miRNA-targeted mRNAs to P-bodies and protects them from decay.

A, B Images generated through confocal microscopy of F-LSM14A^{WT} HeLa cells transfected with plasmids encoding EDC4-V5 after 0 (A) or 4 h (B) of actinomycin D (Act-D) treatment. Fluorescent *in situ* hybridization (FISH) using Cy3-labeled probes against RL-6xB with simultaneous immunofluorescent staining was performed using α-DDX6 with α-FLAG or α-V5 antibodies. Images were processed, analyzed, and channels merged using Fiji.

C Quantification of P-body sizes from experiments depicted in (A, B) with the mean P-body size of control cells with 0 h of Act-D treatment set to 100%. Measurements were performed on three separate biological replicates using Fiji. Error bars represent the SEM and statistical significance was established using a two-tailed Student's *t*-test relative to control conditions (*$P < 0.05$).

D Quantification of total whole-cell FISH signal from the RL-6xB Cy3 channel from experiments depicted in (A, B) with the mean FISH signal of control cells with no Act-D treatment set to 100%. Measurements were performed on three separate biological replicates using Fiji. Error bars represent the SEM and statistical significance was established using a two-tailed Student's *t*-test relative to control conditions (**$P < 0.01$).

E Quantification of the additive FISH signal from all P-bodies as a fraction of the condition-matched total FISH signal from experiments depicted in (A, B). Measurements were performed on three separate biological replicates with 10 cells per replicate using Fiji. Error bars represent the SEM and statistical significance was established using a two-tailed Student's *t*-test relative to control conditions (***$P < 0.001$).

F Quantification of the additive FISH signal per individual P-body as a fraction of the condition-matched total FISH signal from experiments depicted in (A, B). Measurements were performed on three separate biological replicates with 10 cells per replicate using Fiji. Error bars represent the SEM and statistical significance was established using a two-tailed Student's *t*-test (*$P < 0.05$; ***$P < 0.001$).

Source data are available online for this figure.

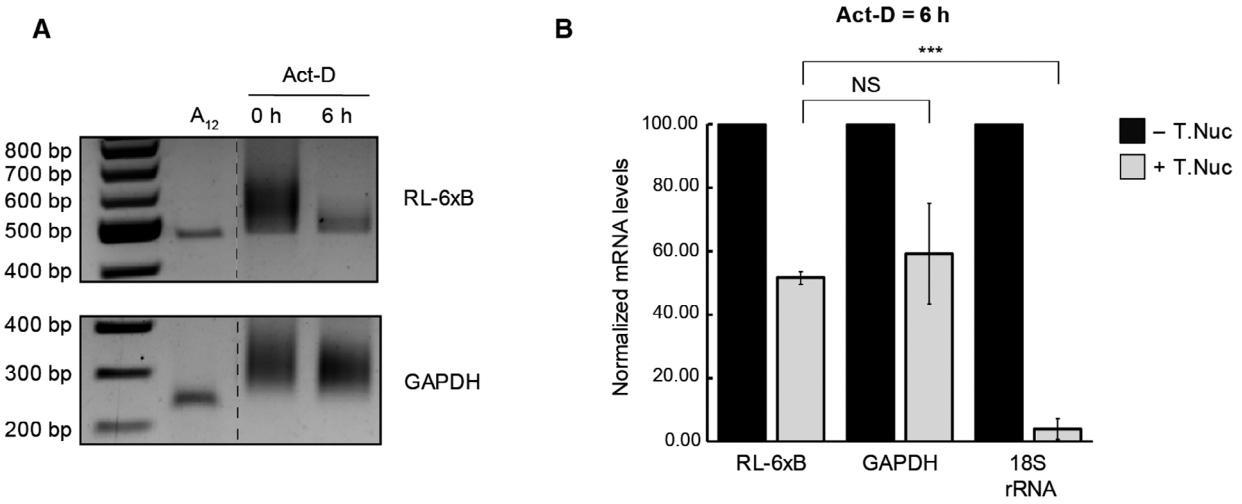

Figure 5. P-body condensates uncouple deadenylation from mRNA decapping.

A Poly(A) tail analyses using an enhanced poly(A)-tailing (ePAT) assay performed on RNA isolated from HeLa cells overexpressing EDC4 and treated with actinomycin D (Act-D) for 0 or 6 h. A_{12} represents ePAT assays performed on mRNAs that have fixed-length 12-adenine tails.

B Cap status analysis of mRNAs collected from HeLa cells overexpressing EDC4 after 6-h of Act-D treatment. Isolated RNA was incubated *in vitro* with terminator nuclease (T. Nuc) along with no-enzyme controls. Purified RNA underwent RT–qPCR analysis for the annotated genes normalized to an *in vitro*-transcribed *firefly luciferase* mRNA spike-in control introduced at the RT step. Normalized mRNA levels of no-enzyme control samples were set to 100%, error bars represent the SEM of three biological replicates, and statistical significance was established using a two-tailed Student's *t*-test (NS = not significant; ***$P < 0.001$).

Source data are available online for this figure.

decapping in *Drosophila* S2 cells (Braun *et al*, 2012). However, this interaction is not conserved in vertebrates, where XRN1 instead directly binds EDC4 (Braun *et al*, 2012). While a recent study suggests XRN1 may interact with the N-terminus of EDC4 (Bloch *et al*, 2023), several reports have shown that XRN1 directly binds to the C-terminal α-helical domain of EDC4, a region that has been reported to oligomerize with other EDC4 proteins and is required for P-body formation (Braun *et al*, 2012; Chang *et al*, 2014; Brothers *et al*, 2022). In keeping with what we observed upon XRN1 depletion, our results indicate that overexpressing EDC4 leads to larger P-bodies that inhibit decapping activity. This suggests that reducing the amount of XRN1 bound to EDC4—either by depleting XRN1 or by increasing EDC4 levels—is what dictates P-body size and decapping activity, potentially by increasing the rate of EDC4 oligomerization. This raises the possibility that EDC4 may respond to changes in XRN1 levels by enhancing P-body formation as a feedback mechanism to block untimely or unwanted mRNA decapping and decay. This could occur under conditions where the decapping complex subunit levels change dramatically, or when XRN1 levels simply cannot keep up with the number of mRNAs that are targeted for decay. However, more research is needed to provide additional support for such a model.

Studies from the Bartel Lab have shown that miRNAs predominantly act in mammalian cells by destabilizing their target mRNAs (Guo *et al*, 2010). Interestingly, we observe that enhancing P-body formation acts to stabilize miRNA-targeted mRNAs by blocking decapping. Importantly, we do not observe changes in the protein outputs produced by these stabilized mRNAs. Rather, our data

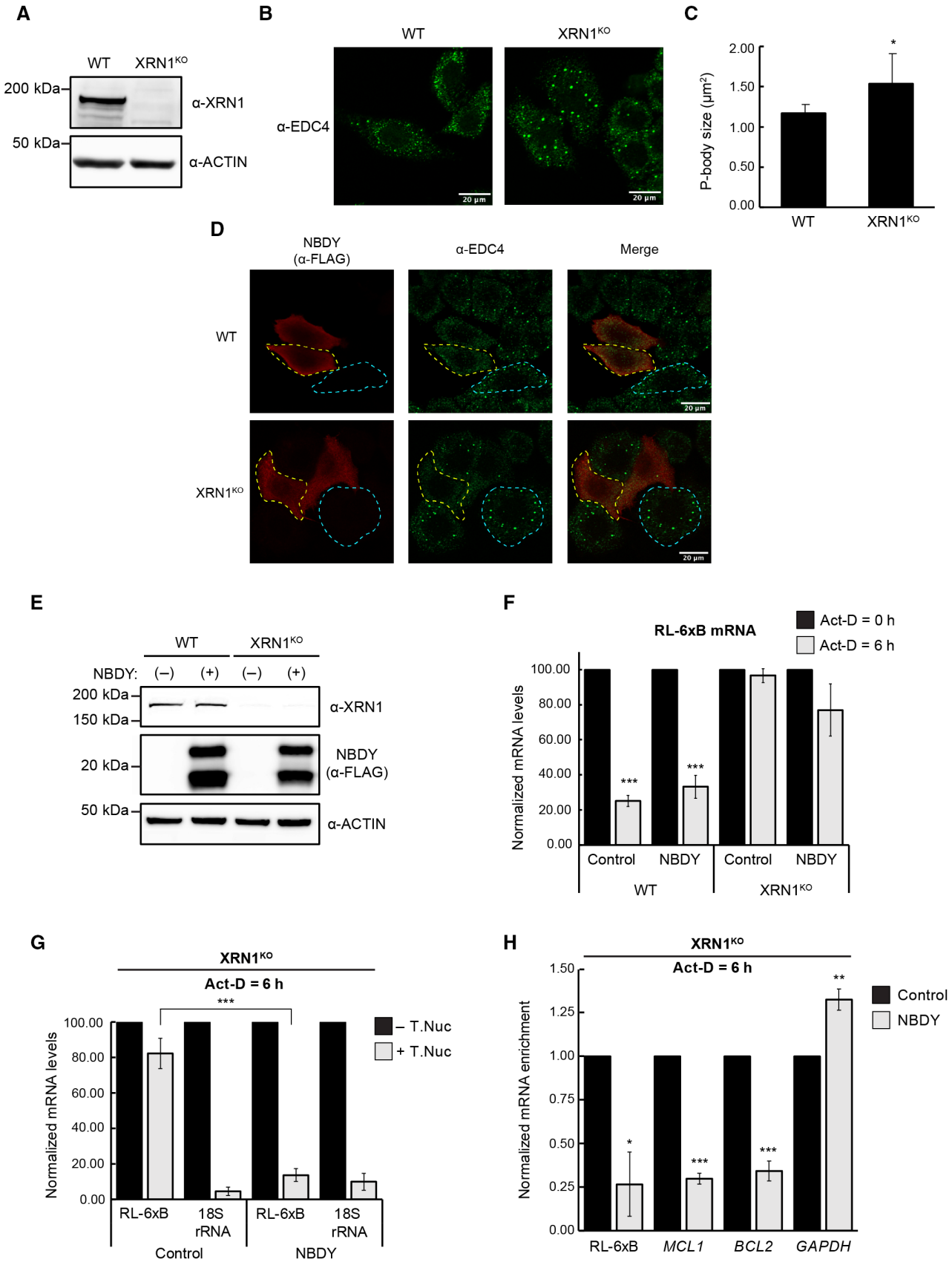

Figure 6.

Figure 6. XRN1 levels modulate P-body formation and regulate mRNA decapping.

A Western blot analysis of XRN1^{KO} HeLa cells generated with CRISPR/Cas9.

B Images generated through confocal microscopy of WT and XRN1^{KO} HeLa cells. Immunofluorescent staining was performed using α-EDC4 to detect P-bodies. Images were processed, and channels were merged using Fiji.

C Quantification of P-body sizes of WT and XRN1^{KO} HeLa cells. Measurements were performed on three separate biological replicates with 10 cells per replicate using Fiji. Error bars represent the SEM and statistical significance was established using a two-tailed Student's *t*-test (*$P < 0.05$).

D Western blot analysis of WT and XRN1^{KO} HeLa cells transfected with plasmid-encoding FLAG-tagged NBDY.

E Images generated through confocal microscopy of WT and XRN1^{KO} HeLa cells transfected with plasmid-encoding FLAG-tagged NBDY. Immunofluorescent staining was performed using α-FLAG and α-EDC4. Transfected cells are outlined in yellow to contrast P-body formation with non-transfected cells (blue outlines). Images were processed, and channels merged using Fiji.

F mRNA decay analysis of WT and XRN1^{KO} HeLa cells transfected with plasmid-encoding FLAG-tagged NBDY. RNA was isolated from cells after treatment with actinomycin D (Act-D) to halt transcription. mRNA levels were measured by RT–qPCR with RL-6xB levels being normalized to *GAPDH* levels. Normalized RL-6xB levels at 0 h of Act-D treatment were set to 100%. Error bars represent the SEM of three biological replicates and statistical significance was established using a two-tailed Student's *t*-test compared to 0-h conditions (***$P < 0.001$).

G Cap status analysis of mRNAs collected from XRN1^{KO} HeLa cells transfected with control plasmids or encoding FLAG-tagged NBDY after 6 h of Act-D treatment. Isolated RNA was incubated *in vitro* with terminator nuclease (T. Nuc) along with no-enzyme control samples. Purified RNA underwent RT–qPCR analysis for the annotated genes normalized to an *in vitro*-transcribed *firefly luciferase* mRNA spike-in control introduced at the RT step. Normalized mRNA levels of no-enzyme control samples were set to 100%, error bars represent the SEM of three biological replicates, and statistical significance was established using a two-tailed Student's *t*-test relative to control (***$P < 0.001$).

H m^7G-cap RNA immunoprecipitations of the indicated mRNAs in Act-D-treated XRN1^{KO} cells expressing GFP (control) or NBDY. Levels of immunopurified mRNAs harboring m^7G-caps were measured by RT–qPCR, normalized to 18S rRNA. mRNA enrichment relative to inputs was set to 100% for control samples, error bars represent the SEM of three biological replicates, and statistical significance was established using a two-tailed Student's *t*-test relative to control (*$P < 0.05$; **$P < 0.01$; ***$P < 0.001$).

Source data are available online for this figure.

suggest that P-body remodeling shifts the mode of mRNA silencing from decay to translational repression. This is consistent with observations that P-body-enriched mRNAs tend to be poorly translated and that P-bodies do not contain ribosomal proteins (Hubstenberger *et al*, 2017; Youn *et al*, 2018; Matheny *et al*, 2019). Indeed, single-molecule imaging studies of reporter mRNAs tethered by the miRNA machinery suggest that P-bodies are sites of persistent translational repression for miRNA-targeted mRNAs (Cialek *et al*, 2022). Notably, the first step in miRNA-mediated mRNA decay involves the recruitment of deadenylases, with deadenylation being associated with translational repression in mammalian cell-free extracts and *Xenopus* oocytes (Fabian *et al*, 2009; Cooke *et al*, 2010; Chekulaeva *et al*, 2011). In agreement with these observations, our results suggest that miRNA-targeted mRNAs stabilized by P-bodies are deadenylated, which may coincide with them being translationally repressed. Although our observations are limited to miRNA-targeted mRNAs, our results are consistent with reports that suggest these observations may hold true for mRNAs that are generally targeted by deadenylation-dependent decay programs. Work from the Lykke-Andersen Lab showed that overexpressing EDC4 in HeLa cells led to the accumulation of a deadenylated reporter mRNA that contains an A/U-rich element (ARE) in its 3′UTR (Fenger-Grøn *et al*, 2005). Moreover, other groups have shown that mRNAs bound by the core P-body protein 4E-T are translationally repressed in a deadenylated state but retain their 5′-caps (Rasch *et al*, 2020). Critically, 4E-T blocked decapping of these mRNAs in a manner that is dependent on whether 4E-T could recruit the cap-binding proteins eIF4E and 4EHP to P-bodies. Several reports across a diverse range of biological contexts suggest that disassembling P-bodies in response to cellular or developmental cues may allow translationally repressed P-body mRNAs to re-initiate their translation (Di Stefano *et al*, 2019; Buddika *et al*, 2021; Sankaranarayanan *et al*, 2021). Thus, it is possible that P-bodies inhibit decapping and recruit the cap-binding protein eIF4E so that P-body-enriched mRNAs can undergo a pioneering round of translation before being decayed in biological or developmental contexts where P-bodies dissolve. However, this hypothesis has not been directly tested.

Figure 7. The EDC4-XRN1 interaction remodels P-bodies to regulate mRNA decapping.

A Schematic diagram of human XRN1, along with diagrams representing deletion mutants expressed in the following experiments.

B mRNA decay analysis of XRN1^{KO} HeLa cells transfected with plasmids encoding the annotated FLAG-tagged XRN1 proteins. RNA was isolated from cells after treatment with actinomycin D (Act-D) to halt transcription. mRNA levels were measured by RT–qPCR with RL-6xB levels being normalized to *GAPDH* levels. Normalized RL-6xB levels at 0 h of Act-D treatment were set to 100%. Error bars represent the SEM of three biological replicates and statistical significance was established using a two-tailed Student's *t*-test relative to control conditions after 6 h of Act-D treatment (*$P < 0.05$; **$P < 0.01$).

C Images generated through confocal microscopy of XRN1^{KO} HeLa cells transfected with plasmids encoding the annotated FLAG-tagged XRN1 proteins. Immunofluorescent staining was performed using α-FLAG and α-EDC4. Transfected cells are outlined in yellow to contrast P-body formation with non-transfected cells (blue outlines). Images were processed, and channels were merged using Fiji.

D Cap status analysis of mRNAs collected from XRN1^{KO} HeLa cells transfected with plasmids encoding FLAG-tagged XRN1 proteins after 6 h of Act-D treatment. Isolated RNA was incubated *in vitro* with terminator nuclease (T. Nuc) along with no-enzyme control samples. Purified RNA underwent RT–qPCR analysis for the annotated genes normalized to an *in vitro*-transcribed *firefly luciferase* mRNA spike-in control introduced at the RT step. Normalized mRNA levels of no-enzyme control samples were set to 100%, error bars represent the SEM of three biological replicates, and statistical significance was established using a two-tailed Student's *t*-test relative to control samples incubated with T. Nuc (*$P < 0.05$).

Source data are available online for this figure.

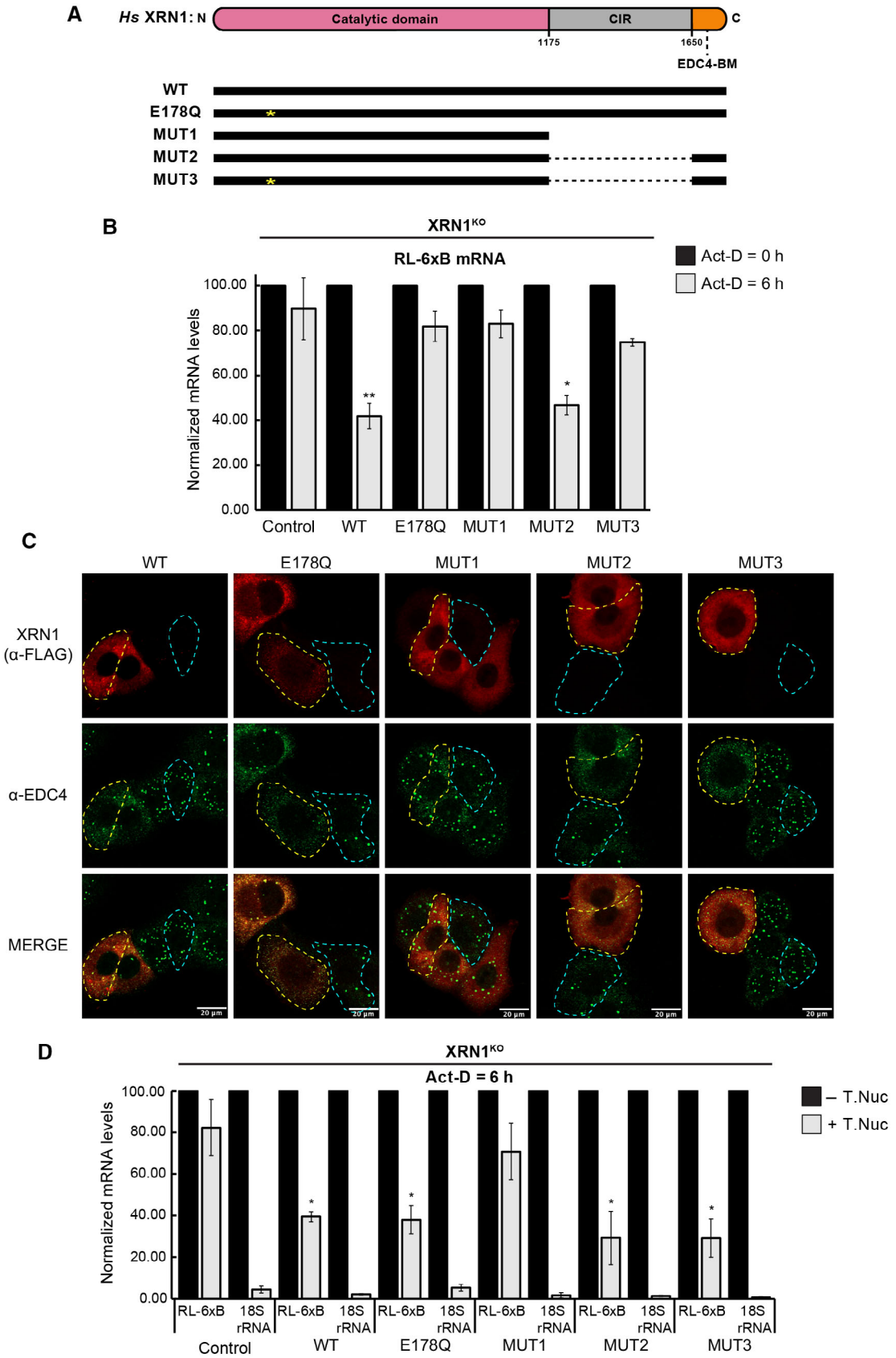

Figure 7.

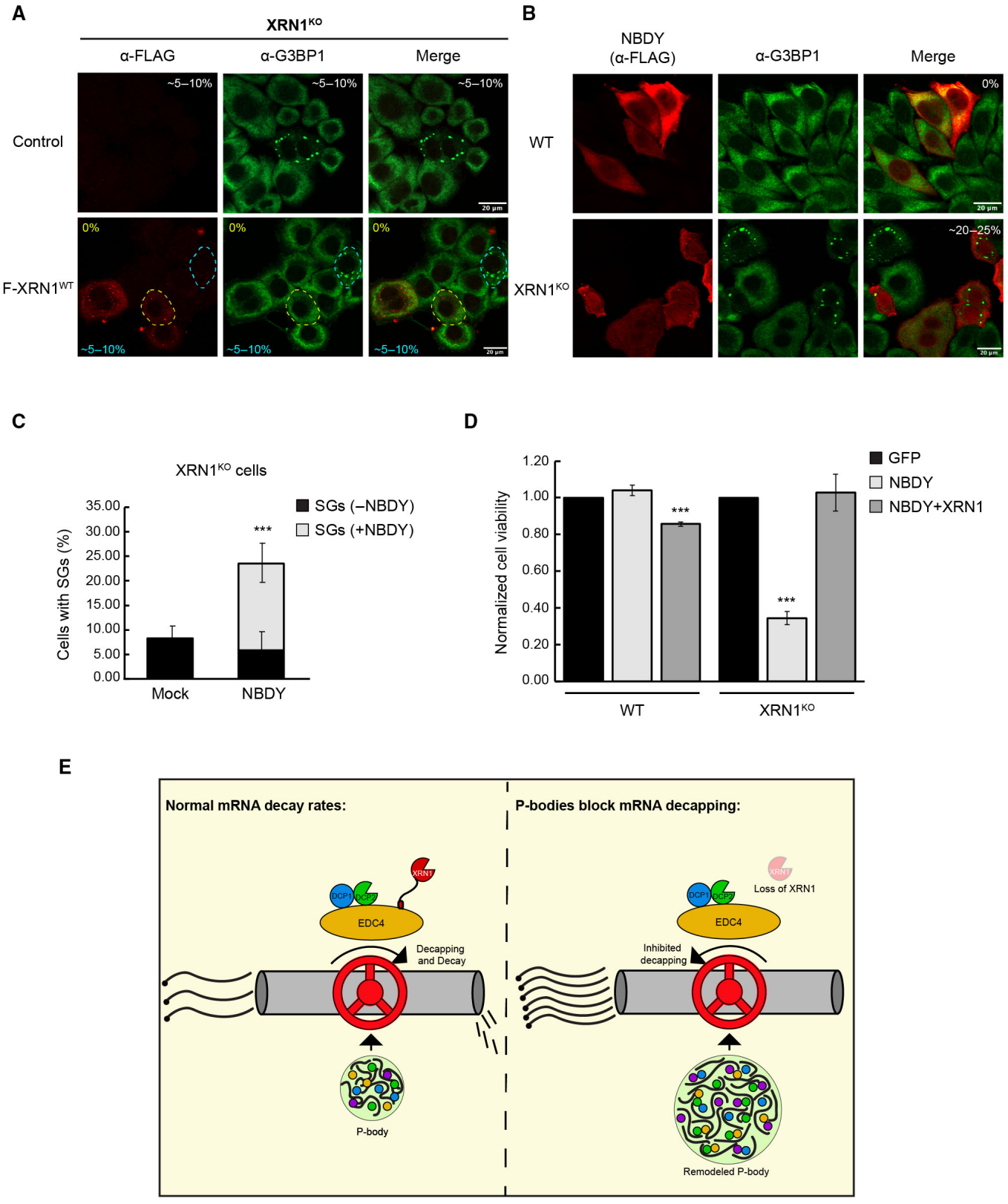

Figure 8.

Figure 8. P-bodies block stress granule formation and support cellular fitness in XRN1^{KO} cells.

A Images generated through confocal microscopy of XRN1^{KO} HeLa cells transfected with or without plasmids encoding the annotated FLAG-tagged XRN1^{WT}. Immunofluorescent staining was performed using α-FLAG and α-G3BP1. Transfected cells are outlined in yellow to contrast stress granule formation (0%) with non-transfected cells (blue outlines; 5–10%). Images were processed, and channels were merged using Fiji.

B Images generated through confocal microscopy of WT or XRN1^{KO} HeLa cells transfected with or without plasmids encoding the annotated FLAG-tagged NBDY. Immunofluorescent staining was performed using α-FLAG and α-G3BP1. The percentage of cells displaying stress granules is annotated under each condition. Images were processed, and channels were merged using Fiji.

C Quantification of the percentage of cells that form stress granules in XRN1^{KO} cells under mock transfection and NBDY transfection conditions. Black bars indicate the percentage of cells with stress granules that occur under control conditions (left) or negative for FLAG-NBDY staining (right), with the gray bar indicating the percentage of cells with SGs that stained positive for FLAG-NBDY expression. Error bars represent the SEM of three biological replicates and statistical significance was determined using a two-tailed Student's *t*-test relative to mock transfection (***$P < 0.001$).

D Fluorometric cell viability analysis of WT and XRN1^{KO} cells transfected with plasmids encoding the indicated proteins. Cell viability was normalized to 1.0 for cells expressing GFP control plasmids. Error bars represent the SEM of three biological replicates and statistical significance was determined using a two-tailed Student's *t*-test relative to GFP control cells (***$P < 0.001$).

E Model representing how P-bodies respond to the loss of XRN1 to regulate mRNA decapping and promote cellular fitness.

Source data are available online for this figure.

While disrupting P-body formation has not been previously linked to impacting cell viability, our data here point to P-bodies supporting cell fitness. Expressing NBDY in XRN1^{KO} cells not only disrupted P-bodies but also led to the formation of stress granules and a concomitant decrease in cell viability. Interestingly, while we were able to generate XRN1^{KO} or LSM14A^{KO} cell lines (the latter of which fails to form visible P-bodies), we were unable to generate homozygous XRN1/LSM14A double knockouts in either genetic background. This suggests that loss of both XRN1 and P-body formation may confer a synthetic lethal phenotype. Preventing P-bodies from forming may lead to a build-up of stable decapped mRNAs in cells lacking XRN1. As these transcripts would theoretically be unable to initiate translation in the absence of their 5′-caps, it is possible that they could act to nucleate stress granules in the absence of stress. Nevertheless, exactly how P-bodies buffer stress granule formation and support cell viability in the absence of XRN1 remain to be elucidated.

In conclusion, our results show that P-bodies dynamically regulate mRNA decapping in response to changes in decapping complex stoichiometry and association. Moreover, our work suggests that P-bodies buffer stress granule formation and support cellular fitness in the absence of XRN1. Future research will be needed to understand how P-bodies can compensate for disrupted 5′ to 3′ decay to support cellular viability and when this may occur.

Materials and Methods

Cell lines and cell culture

We obtained epithelioid carcinoma HeLa cells from ATCC. Cell lines were identified via morphology but have not been authenticated. Cells were assessed and tested negative for mycoplasma contamination. HeLa cells were grown in Dulbecco's modified Eagle's medium (DMEM) supplemented with 10% fetal bovine serum, 50 U/ml penicillin, and 50 mg/ml streptomycin. FLAG-LSM14A complementation cell lines were generated as previously described (Brandmann *et al*, 2018).

Plasmids and antibodies

Plasmid transfections were performed using polyethyleneimine (PEI) or Lipofectamine 2000 (Thermo Fisher). V5-tagged EDC4-encoding plasmids were generated by Gateway cloning from pDONR-EDC4 into a pDEST40 vector as previously described (Brothers *et al*, 2020). FLAG-tagged XRN1 constructs were generated by cloning PCR amplicons into pQCXIB using the AgeI and EcoRI sites. FLAG-tagged NBDY was cloned into pcDNA3.1 as previously described (Brothers *et al*, 2022). pCI RL-6xB, RL-6xBMUT, and FL reporter plasmids were also constructed as previously described (Pillai *et al*, 2005; Fabian *et al*, 2009). RL-6xB and RL-6xBMUT reporters were subcloned into a pTRE-tight vector, which along with pTET-OFF plasmids were kindly gifted from Volker Blank. Antibodies for this study were purchased against FLAG (Sigma), V5 (Rabbit—Cell Signaling; Mouse—Thermo Fisher), EDC4 (Bethyl), DDX6 (Bethyl), XRN1 (Bethyl), LSM14 (GeneTex), ACTIN (Sigma), GAPDH (Cell Signaling), m^{7}G (MBL), MCL1 (Santa Cruz), and BCL2 (Cell Signaling). Antibodies used for western blot and immunofluorescence microscopy were diluted to the manufacturer's specifications.

CRISPR-Cas9 gene editing

gRNAs targeting LSM14A (5′-TCTGTACCAAAGGATCGAAC-3′) and XRN1 (5′-AGAGAAGAAGTTCGATTTGG-3′) were cloned into Lenti-CRISPR v2 (Addgene #52961) using BsmBI restriction enzyme sites and confirmed by sequencing. WT HeLa cells were transiently transfected with recombinant LentiCRISPR v2 plasmids followed by puromycin (2 μg/ml) selection 48 h after transfection. Forty-eight hours after selection, cells were returned to normal cell culture medium to recover for 24 additional hours. After selection recovery, cells were plated into 96-well plates, with monoclonal lines being grown up and screened by western blotting for knockouts.

Immunofluorescent and FISH microscopy

Standard immunofluorescent (IF) analyses were performed as previously described (Brothers *et al*, 2022). Concomitant IF and FISH analyses were adapted from Adivarahan *et al* (2018): Previously transfected HeLa cells were plated on coverslips and grown for 12-h to allow them to adhere. Coverslips were washed with 1×PBS and fixed with 4% PFA/1×PBS for 10 min at RT. Coverslips were washed with 1×PBS and then stored in 1 ml of 70% EtOH overnight at −20°C. EtOH was removed and cells were washed with 1×PBS before being air dried for 5 min. This was followed by permeabilization with 0.5% Triton x-100/1×PBS for 10 min at RT and three washes of 1×PBS. Hybridization buffers were prepared as previously described (Adivarahan

et al, 2018) using Cy3-labeled probes complementary to the *Renilla* luciferase CDS (Biosearch/Stellaris). Coverslips were incubated with hybridization buffer for 3 h at 37°C shielded from light. Coverslips were then washed twice with 10% Formamide/2×SSC for 30 min per wash at 37°C shielded from light, followed by three washes with 1×PBS (no incubation). Hybridized coverslips were then blocked with 4% BSA for 10 min at RT followed by an overnight incubation at 4°C with primary antibodies diluted in 1% BSA (shielded from light). After primary antibody incubation, coverslips were washed with 1×PBS and incubated with Alexa Fluor 488 goat anti-rabbit and Alexa Fluor 594 goat anti-mouse antibodies diluted 1:500 in 1% BSA for 45 min at RT (shielded from light). This was followed by washing the coverslips with 1×PBS, and nuclei were stained with DAPI for 15 min at RT (shielded from light). Coverslips were washed with 1×PBS before being mounted onto glass slides with ProLong Gold media (Thermo Fisher). Images were taken using a Zeiss Confocal LSM 800 microscope at 40× magnification and processed with Fiji to merge channels, add scale bars, and quantify FISH signals.

Luciferase assays and mRNA decay assays

HeLa cells were transfected with the indicated plasmids at 30% confluency. Twenty-four hours after transfection, cells were reseeded into six-well dishes for collection at the relevant time points in mRNA decay assays, along with additional wells for luciferase assays. Twenty-four hours later, cells were harvested and lysed in Passive Lysis Buffer (Promega). The activity levels of the *Renilla* (RL) and firefly (FL) luciferase were measured using a Dual-Luciferase Assay (Promega). For mRNA decay assays, cell culture media were replaced with media containing actinomycin D (5 μg/ml) or doxycycline (1 μg/ml) for TET-OFF reporter analyses. Cells were harvested at the indicated time points, pelleted, and flash frozen before being stored at -80°C. Frozen pellets were processed for RT–qPCR analyses as previously described (Brothers *et al*, 2022).

Poly(A) tail analyses

Enhanced poly(A) tail (ePAT) analyses were performed as previously described (Jänicke *et al*, 2012). The anchor primer used in the ePAT reverse transcription step is (5′-GCGAGCTGGCGCCGGCG CTTTTTTTTTTTT-3′). The (dT)12VN primer used in the reverse transcription to generate a size marker for the fixed length A_{12}-tail product is (5′-GCGAGCTGGCGCCGGCGCTTTTTTTTTTTTVN-3′). PCR reactions were then performed using Taq polymerase (Biobasic), resolved on 2% agarose gels stained with EtBr. Gels were visualized using an ImageQuant LAS 4000 imager (GE Healthcare).

Terminator nuclease assays

Purified RNA was incubated with Terminator nuclease and buffer A (Biosearch Technologies) for 1 h at 30°C, according to the manufacturer's specifications. RNA was then resuspended in an equal volume of 3 M NaOAc (pH 5.5) and phenol chloroform extracted. Purified RNA was EtOH precipitated and resuspended in water before undergoing reverse transcription (RT) with an *in vitro* transcribed *firefly luciferase* mRNA spike-in control (0.1 ng per reaction) to normalize for RT efficiency. Quantitative PCR (qPCR) was subsequently performed as described above, except for 18S rRNA analysis where cDNA was diluted 1:1,000 before undergoing qPCR. For recombinant mRNA-decapping enzyme incubation, purified RNA was incubated with mRNA-decapping enzyme and buffer (NEB) for 1 h at 37°C, according to the manufacturer's specifications. RNA was then resuspended in an equal volume of 3 M NaOAc (pH 5.5) and phenol chloroform extracted. Purified RNA was EtOH precipitated and resuspended in water before being divided and incubated with Terminator nuclease, as described above.

Fluorometric cell viability assays

Cells were carefully counted and seeded at equal density. Twenty-four hours after seeding, cells were transfected with plasmids encoding the indicated proteins along with a puromycin selection cassette. Twenty-four hours post-transfection, transfected cells were selected with media containing puromycin (2 μg/ml) and grown for an additional 48-h. Cells were then harvested, stained with acridine orange and propidium iodide, and live cells were counted using CellDrop FL Cell Counter (Denovix).

m^7G-cap RNA immunoprecipitation

Cultured $XRN1^{KO}$ cells were transfected with plasmids encoding RL-6xB reporters, empty puromycin selection cassettes, and plasmids encoding either GFP (control) or FLAG-NBDY. Twenty-four hours after transfection, cells were selected with 2 μg/ml puromycin for 48 h with the final 6 h being co-treated with 5 μg/ml of actinomycin D to halt transcription. Cells were then harvested and total RNA was extracted using an EZ-10 total RNA miniprep kit (Biobasic). Two microgram of input RNA was Turbo DNase treated and kept as input samples. m^7G-cap RNA immunoprecipitations were then performed as previously described (Pandolfini *et al*, 2019): 25 μg of total RNA was incubated in RIP buffer (10 mM Tris–HCl pH 7.4, 150 mM NaCl, and 0.1% NP-40) with 10 μg of anti-m^7G (MBL), and 10 μl of RNase inhibitor for 2 h at 4°C with rotation. Simultaneously, protein G Dynabeads (Thermo Fisher) were washed with RIP buffer and blocked with 1 μg/μl BSA (NEB) for 2 h at 4°C with rotation. Blocked beads were washed with RIP buffer, resuspended, and added to RNA-antibody mixes for an additional 2 h at 4°C with rotation. Bead and RNA solutions were washed thoroughly with RIP buffer and then IP RNA was resuspended in RIP buffer containing 6.7 mM m^7GTP and incubated at 37°C for 30 min to elute mRNAs from the beads. Input and IP RNA were isolated and concentrated using a Qiagen RNeasy kit. RT–qPCR was then performed on input and IP RNA samples as described above. CT values for RL-6xB, *MCL1*, *BCL2*, and *GAPDH* were normalized to 18S rRNA to generate ΔCT values. ΔCTs were transformed into ΔΔCTs by normalizing the IP ΔCT to the input ΔCT. Finally, ΔΔΔCT was calculated by normalizing the NBDY ΔΔCT to control ΔΔCTs. Relative fold enrichment was calculated as $2^{-\Delta\Delta CT}$ and normalized mRNA enrichment was calculated as $2^{-\Delta\Delta\Delta CT}$.

Data availability

This study includes no data deposited in external repositories.

Expanded View for this article is available online.

Acknowledgements

We would like to thank Thomas Duchaine and Selena Sagan for helpful comments; Christine Vande Velde and Hana Fakim for FISH reagents; Volker Blank for select plasmids; and Ivan Topisirovic for MCL1 antibody. This work is supported by a Canadian Institutes of Health Research (CIHR) grant (PJT-156356) and a Natural Sciences and Engineering Research Council of Canada (NSERC) Discovery grant (RGPIN-2022-04215) to MRF; Fonds de Recherche du Québec- Santé (FRQS) Chercheur-Boursier Senior to MRF. WRB is supported by an NSERC CGS-D Alexander Graham Bell scholarship. SK is supported by an NSERC PGS-D scholarship. FA was supported by an NSERC Undergraduate Student Research Award.

Author contributions

William R Brothers: Conceptualization; formal analysis; investigation; writing – original draft; writing – review and editing. **Farah Ali:** Formal analysis. **Sam Kajjo:** Investigation; methodology. **Marc R Fabian:** Conceptualization; supervision; writing – original draft; writing – review and editing.

Disclosure and competing interests statement

The authors declare that they have no conflict of interest.

References

Adivarahan S, Livingston N, Nicholson B, Rahman S, Wu B, Rissland OS, Zenklusen D (2018) Spatial organization of single mRNPs at different stages of the gene expression pathway. *Mol Cell* 72: 727 – 738

Aizer A, Kafri P, Kalo A, Shav-Tal Y (2013) The P body protein Dcp1a is hyper-phosphorylated during mitosis. *PloS One* 8: e49783

Arribere JA, Doudna JA, Gilbert WV (2011) Reconsidering movement of eukaryotic mRNAs between polysomes and P bodies. *Mol Cell* 44: 745 – 758

Beckham CJ, Parker R (2008) P bodies, stress granules, and viral life cycles. *Cell Host Microbe* 3: 206 – 212

Bloch DB, Sinow CO, Sauer AJ, Corman BHP (2023) Assembly and regulation of the mammalian mRNA processing body. *PloS One* 18: e0282496

Brandmann T, Fakim H, Padamsi Z, Youn JY, Gingras AC, Fabian MR, Jinek M (2018) Molecular architecture of LSM14 interactions involved in the assembly of mRNA silencing complexes. *EMBO J* 37: e97869

Brangwynne CP, Eckmann CR, Courson DS, Rybarska A, Hoege C, Gharakhani J, Jülicher F, Hyman AA (2009) Germline P granules are liquid droplets that localize by controlled dissolution/condensation. *Science* 324: 1729 – 1732

Braun JE, Huntzinger E, Fauser M, Izaurralde E (2011) GW182 proteins directly recruit cytoplasmic deadenylase complexes to miRNA targets. *Mol Cell* 44: 120 – 133

Braun JE, Truffault V, Boland A, Huntzinger E, Chang CT, Haas G, Weichenrieder O, Coles M, Izaurralde E (2012) A direct interaction between DCP1 and XRN1 couples mRNA decapping to 5′ exonucleolytic degradation. *Nat Struct Mol Biol* 19: 1324 – 1331

Brothers WR, Hebert S, Kleinman CL, Fabian MR (2020) A non-canonical role for the EDC4 decapping factor in regulating MARF1-mediated mRNA decay. *Elife* 9: e54995

Brothers WR, Fakim H, Kajjo S, Fabian MR (2022) P-bodies directly regulate MARF1-mediated mRNA decay in human cells. *Nucleic Acids Res* 50: 7623 – 7636

Buddika K, Huang YT, Ariyapala IS, Butrum-Griffith A, Norrell SA, O'Connor AM, Patel VK, Rector SA, Slovan M, Sokolowski M *et al* (2021) Coordinated repression of pro-differentiation genes via P-bodies and transcription maintains *Drosophila* intestinal stem cell identity. *Curr Biol* 32: 386 – 397

Chang JH, Xiang S, Xiang K, Manley JL, Tong L (2011) Structural and biochemical studies of the 5′→3′ exoribonuclease Xrn1. *Nat Struct Mol Biol* 18: 270 – 276

Chang C-T, Bercovich N, Loh B, Jonas S, Izaurralde E (2014) The activation of the decapping enzyme DCP2 by DCP1 occurs on the EDC4 scaffold and involves a conserved loop in DCP1. *Nucleic Acids Res* 42: 5217 – 5233

Chang CT, Muthukumar S, Weber R, Levdansky Y, Chen Y, Bhandari D, Igreja C, Wohlbold L, Valkov E, Izaurralde E (2019) A low-complexity region in human XRN1 directly recruits deadenylation and decapping factors in 5′-3′ messenger RNA decay. *Nucleic Acids Res* 47: 9282 – 9295

Chekulaeva M, Mathys H, Zipprich JT, Attig J, Colic M, Parker R, Filipowicz W (2011) miRNA repression involves GW182-mediated recruitment of CCR4-NOT through conserved W-containing motifs. *Nat Struct Mol Biol* 18: 1218 – 1226

Chen CY, Ezzeddine N, Shyu AB (2008) Messenger RNA half-life measurements in mammalian cells. *Methods Enzymol* 448: 335 – 357

Cialek CA, Galindo G, Morisaki T, Zhao N, Montgomery TA, Stasevich TJ (2022) Imaging translational control by Argonaute with single-molecule resolution in live cells. *Nat Commun* 13: 3345

Collart MA, Panasenko OO (2012) The Ccr4–not complex. *Gene* 492: 42 – 53

Cooke A, Prigge A, Wickens M (2010) Translational repression by deadenylases. *J Biol Chem* 285: 28506 – 28513

Cougot N, Babajko S, Seraphin B (2004) Cytoplasmic foci are sites of mRNA decay in human cells. *J Cell Biol* 165: 31 – 40

Cui J, Placzek WJ (2018) PTBP1 enhances miR-101-guided AGO2 targeting to MCL1 and promotes miR-101-induced apoptosis. *Cell Death Dis* 9: 552

Di Stefano B, Luo E-C, Haggerty C, Aigner S, Charlton J, Brumbaugh J, Ji F, Rabano Jiménez I, Clowers KJ, Huebner AJ *et al* (2019) The RNA helicase DDX6 controls cellular plasticity by modulating P-body homeostasis. *Cell Stem Cell* 25: 622 – 638

D'Lima NG, Ma J, Winkler L, Chu Q, Loh KH, Corpuz EO, Budnik BA, Lykke-Andersen J, Saghatelian A, Slavoff SA (2017) A human microprotein that interacts with the mRNA decapping complex. *Nat Chem Biol* 13: 174 – 180

Erickson SL, Corpuz EO, Maloy JP, Fillman C, Webb K, Bennett EJ, Lykke-Andersen J (2015) Competition between decapping complex formation and ubiquitin-mediated proteasomal degradation controls human Dcp2 decapping activity. *Mol Cell Biol* 35: 2144 – 2153

Eulalio A, Behm-Ansmant I, Izaurralde E (2007a) P bodies: at the crossroads of post-transcriptional pathways. *Nat Rev Mol Cell Biol* 8: 9 – 22

Eulalio A, Behm-Ansmant I, Schweizer D, Izaurralde E (2007b) P-body formation is a consequence, not the cause, of RNA-mediated gene silencing. *Mol Cell Biol* 27: 3970 – 3981

Fabian MR, Mathonnet G, Sundermeier T, Mathys H, Zipprich JT, Svitkin YV, Rivas F, Jinek M, Wohlschlegel J, Doudna JA *et al* (2009) Mammalian miRNA RISC recruits CAF1 and PABP to affect PABP-dependent deadenylation. *Mol Cell* 35: 868 – 880

Fabian MR, Sonenberg N, Filipowicz W (2010) Regulation of mRNA translation and stability by microRNAs. *Annu Rev Biochem* 79: 351 – 379

Fenger-Grøn M, Fillman C, Norrild B, Lykke-Andersen J (2005) Multiple processing body factors and the ARE binding protein TTP activate mRNA decapping. *Mol Cell* 20: 905 – 915

Franks TM, Lykke-Andersen J (2008) The control of mRNA decapping and P-body formation. *Mol Cell* 32: 605 – 615

Guo H, Ingolia NT, Weissman JS, Bartel DP (2010) Mammalian microRNAs predominantly act to decrease target mRNA levels. *Nature* 466: 835 – 840

Hubstenberger A, Courel M, Benard M, Souquere S, Ernoult-Lange M, Chouaib R, Yi Z, Morlot JB, Munier A, Fradet M *et al* (2017) P-body purification

reveals the condensation of repressed mRNA regulons. *Mol Cell* 68: 144 – 157

Ishimaru D, Zuraw L, Ramalingam S, Sengupta TK, Bandyopadhyay S, Reuben A, Fernandes DJ, Spicer EK (2010) Mechanism of regulation of bcl-2 mRNA by nucleolin and A+U-rich element-binding factor 1 (AUF1). *J Biol Chem* 285: 27182 – 27191

Jänicke A, Vancuylenberg J, Boag PR, Traven A, Beilharz TH (2012) ePAT: a simple method to tag adenylated RNA to measure poly(A)-tail length and other 3' RACE applications. *RNA* 18: 1289 – 1295

Jonas S, Izaurralde E (2013) The role of disordered protein regions in the assembly of decapping complexes and RNP granules. *Genes Dev* 27: 2628 – 2641

Jonas S, Izaurralde E (2015) Towards a molecular understanding of microRNA-mediated gene silencing. *Nat Rev Genet* 16: 421 – 433

Liu J, Valencia-Sanchez MA, Hannon GJ, Parker R (2005) MicroRNA-dependent localization of targeted mRNAs to mammalian P-bodies. *Nat Cell Biol* 7: 719 – 723

Luo Y, Na Z, Slavoff SA (2018) P-bodies: composition, properties, and functions. *Biochemistry* 57: 2424 – 2431

Luo Y, Schofield JA, Simon MD, Slavoff SA (2020) Global profiling of cellular substrates of human Dcp2. *Biochemistry* 59: 4176 – 4188

Matheny T, Rao BS, Parker R (2019) Transcriptome-wide comparison of stress granules and P-bodies reveals that translation plays a major role in RNA partitioning. *Mol Cell Biol* 39: e00313-19

Na Z, Luo Y, Schofield JA, Smelyansky S, Khitun A, Muthukumar S, Valkov E, Simon MD, Slavoff SA (2020) The NBDY microprotein regulates cellular RNA decapping. *Biochemistry* 59: 4131 – 4142

Na Z, Luo Y, Cui DS, Khitun A, Smelyansky S, Loria JP, Slavoff SA (2021) Phosphorylation of a human microprotein promotes dissociation of biomolecular condensates. *J Am Chem Soc* 143: 12675 – 12687

Pandolfini L, Barbieri I, Bannister AJ, Hendrick A, Andrews B, Webster N, Murat P, Mach P, Brandi R, Robson SC *et al* (2019) METTL1 promotes let-7 microRNA processing via m7G methylation. *Mol Cell* 74: 1278 – 1290

Paquette DR, Mugridge JS, Weinberg DE, Gross JD (2018) Application of a *Schizosaccharomyces pombe* Edc1-fused Dcp1-Dcp2 decapping enzyme for transcription start site mapping. *RNA* 24: 251 – 257

Parker R, Sheth U (2007) P bodies and the control of mRNA translation and degradation. *Mol Cell* 25: 635 – 646

Pillai RS, Bhattacharyya SN, Artus CG, Zoller T, Cougot N, Basyuk E, Bertrand E, Filipowicz W (2005) Inhibition of translational initiation by Let-7 microRNA in human cells. *Science* 309: 1573 – 1576

Protter DSW, Parker R (2016) Principles and properties of stress granules. *Trends Cell Biol* 26: 668 – 679

Rasch F, Weber R, Izaurralde E, Igreja C (2020) 4E-T-bound mRNAs are stored in a silenced and deadenylated form. *Genes Dev* 34: 847 – 860

Sankaranarayanan M, Emenecker RJ, Wilby EL, Jahnel M, Trussina I, Wayland M, Alberti S, Holehouse AS, Weil TT (2021) Adaptable P body physical states differentially regulate bicoid mRNA storage during early *Drosophila* development. *Dev Cell* 56: 2886 – 2901

Sheth U, Parker R (2003) Decapping and decay of messenger RNA occur in cytoplasmic processing bodies. *Science* 300: 805 – 808

Standart N, Weil D (2018) P-bodies: cytosolic droplets for coordinated mRNA storage. *Trends Genet* 34: 612 – 626

Tibble RW, Depaix A, Kowalska J, Jemielity J, Gross JD (2021) Biomolecular condensates amplify mRNA decapping by biasing enzyme conformation. *Nat Chem Biol* 17: 615 – 623

Urlinger S, Baron U, Thellmann M, Hasan MT, Bujard H, Hillen W (2000) Exploring the sequence space for tetracycline-dependent transcriptional activators: novel mutations yield expanded range and sensitivity. *Proc Natl Acad Sci USA* 97: 7963 – 7968

Vidya E, Duchaine TF (2022) Eukaryotic mRNA decapping activation. *Front Genet* 13: 832547

Yamashita A, Chang T-C, Yamashita Y, Zhu W, Zhong Z, Chen C-YA, Shyu A-B (2005) Concerted action of poly(A) nucleases and decapping enzyme in mammalian mRNA turnover. *Nat Struct Mol Biol* 12: 1054 – 1063

Youn JY, Dunham WH, Hong SJ, Knight JDR, Bashkurov M, Chen GI, Bagci H, Rathod B, MacLeod G, Eng SWM *et al* (2018) High-density proximity mapping reveals the subcellular organization of mRNA-associated granules and bodies. *Mol Cell* 69: 517 – 532